Charm production in hadronic and heavy-ion collisions at ultrarelativistic energies to $O(\alpha_s^3)$

Ina Sarcevic and Peter Valerio
Department of Physics, University of Arizona, Tucson, Arizona 85721
(Received 15 November 1994)

We present results on rapidity and transverse momentum distributions of inclusive charm quark production in hadronic and heavy-ion collisions at RHIC and LHC energies, including the next-to-leading order $O(\alpha_s^3)$, radiative corrections, and the nuclear shadowing effect. We determine the hadronic and the *effective* (in-medium) K factor for the differential and total inclusive charm cross sections. We find the fraction of central and inelastic events that contain at least one charm quark pair at LHC energies and obtain the effective A dependence of the inclusive charm production in proton-nucleus and nucleus-nucleus collisions at RHIC and in nucleus-nucleus collisions at the LHC. We discuss theoretical uncertainties inherent in our calculation. In particular, we show how different extrapolations of gluon density in a nucleon *and* in a nucleus to the low-x region introduce large theoretical uncertainty in the calculation of charm production at LHC energies.

PACS number(s): 25.75.+r, 14.40.Lb, 24.85.+p

I. INTRODUCTION

Recently, there is a considerable theoretical and experimental interest in studying charm production in hadronic and nuclear collisions. Theoretical calculation of the heavy-quark differential and total cross sections has been improved by including the next-to-leading order, $O(\alpha_s^3)$, radiative corrections [1,2]. For bottom and charm production these corrections are large, especially at threshold energies and at very high energies. Future high-precision measurements of the charm production at Fermilab fixed-target experiments could therefore provide a stringent test of perturbative QCD [3]. In addition, studying charm production at the proposed heavy-ion colliders, BNL's Relativistic Heavy Ion Collider (RHIC) and CERN's Large Hadron Collider (LHC) is of special interest. Open charm production has been suggested as an elegant signal for detecting the formation of quark-gluon plasma (QGP) in heavy-ion collisions [4]. If thermalization is reached in heavy-ion collisions at RHIC and LHC, we expect a very dense matter, of the order of few GeV/fm^3, to be formed in the initial stage of the collision. It seems plausible that this density is sufficient for creating a new state of matter, the QGP [5]. The search for a clean, detectable signal for this new state of matter has been one of the most challenging theoretical problems for the last few years. Some of the proposed signals, thermal photons, dileptons, and J/Ψ suppression have been studied and found to be difficult to detect due to the large QCD background [6]. In order that the enhanced charm production can be used as the signal of QGP, we need to understand the QCD background, namely the production of charm quarks through the hard collisions of partons inside the nuclei. This type of charm production at RHIC and LHC energies is dominated by initial-state gluons. Therefore, in addition to the possibility of pointing towards the formation of quark-gluon plasma in high-energy heavy-ion collisions, combined measurements of charm production in p-p, p-A, and A-A collisions could provide valuable information about the gluon density in a nucleus.

In Sec. II, we present our calculation of the total cross section for open charm production in hadronic collisions and compare our results with the low-energy measurements. Our calculation includes the next-to-leading order, $O(\alpha_s^3)$, radiative corrections. We discuss theoretical uncertainties due to the choice of the factorization and renormalization scale and the choice of the parton structure function. We show how the low-energy measurements of the total cross section for charm production in p-p and p-A collisions provide certain constraints on our theoretical parameters. We illustrate the importance of including the next-to-leading order corrections at these energies. We present our predictions for the total cross section for charm production in p-p collisions at RHIC and LHC energies. In Sec. III, we review nuclear effects of relevance to charm production in nuclear collisions. In particular, we obtain the number of nucleon-nucleon collisions per unit transverse area at fixed impact parameter, the so-called spatial overlapping function, for two different choices of the nuclear density, the Woods-Saxon [7] and the Gaussian form. We also discuss the nuclear shadowing effect in the standard parton model and recent direct measurements of this effect on quark distribution in a nucleus. We find the effective A dependence of the total cross section for charm production in A-A collisions at RHIC and LHC and determine the fraction of central and inelastic events that contains at least one charm quark pair at these energies. In Sec. IV, we present rapidity and transverse momentum distributions for charm production in hadronic and nuclear collisions. We illustrate the importance of the $O(\alpha_s^3)$ corrections *combined* with nuclear shadowing effects in different regions of phase space by calculating the *effective* (i.e., in-medium) K factor, defined as the ratio of the inclusive distribution for charm production in A-A collisions to the leading-order distribution without nuclear effects. We show that the K factor, in general, is a function of rapidity, transverse momentum, and x_F ($x_F = p_z/p_{z\,\max}$, and p_z is taken to be in the beam direction) and can-

not be taken to be a constant. In Sec. V we present our conclusions.

II. THE TOTAL CROSS SECTION FOR CHARM PRODUCTION IN HADRONIC COLLISIONS

In perturbative QCD, the total inclusive cross section for charm production in hadronic collisions is obtained as a convolution of parton densities in the hadron with the hard scattering cross section. Our calculation includes both the leading-order subprocesses, $O(\alpha_s^2)$, such as $q+\bar{q} \to Q+\bar{Q}$ and $g+g \to Q+\bar{Q}$, and next-to-leading order subprocesses, $O(\alpha_s^3)$, such as $q+\bar{q} \to Q+\bar{Q}+g$, $g+q \to Q+\bar{Q}+g$, $g+\bar{q} \to Q+\bar{Q}+\bar{q}$, and $g+g \to Q+\bar{Q}+g$. The total inclusive cross section for charm production in hadronic collisions can be written as

$$\sigma_c = \int_{4m_c^2/s}^1 dx_a \int_{4m_c^2/x_a s}^1 dx_b \sum_{i,j}^{\text{partons}} [F_i(x_a,Q^2)F_j(x_b,Q^2)\hat{\sigma}_{i,j}(\hat{s},m_c^2,Q^2)] \ , \tag{1}$$

where the $F_i(x,Q^2)$'s are the parton distributions in a nucleon, x_a and x_b are the fractional momenta of incoming partons and $\hat{s}=x_a x_b s$ is the parton-parton center-of-mass energy. The parton cross section $\hat{\sigma}_{i,j}(\hat{s},m_c^2,Q^2)$ has been calculated to the order $O(\alpha_s^3)$ and can be written as

$$\hat{\sigma}_{i,j}(\hat{s},m_c^2,Q^2) = \frac{\alpha_s^2(Q^2)}{m_c^2} f_{i,j}\left(\rho,\frac{Q^2}{m_c^2}\right) \ , \tag{2}$$

where

$$f_{i,j}(\rho,Q^2/m_c^2) = f_{i,j}^{(0)}(\rho) + 4\pi\alpha_s(Q^2)[f_{i,j}^{(1)}(\rho) + \bar{f}_{i,j}^{(1)}(\rho)\ln(Q^2/m_c^2)] \ . \tag{3}$$

The functions $f_{i,j}^{(0)}$, $f_{i,j}^{(1)}$, and $\bar{f}_{i,j}^{(1)}$ are given in Ref. [1]. The coupling constant $\alpha_s(Q^2)$, calculated to next-to-leading order, is given by

$$\alpha_s(Q^2) = \frac{12\pi}{(33-2N_f)\ln(Q^2/\Lambda^2)}\left(1-\frac{6(153-19N_f)\ln\ln Q^2/\Lambda^2}{(33-2N_f)^2\ln Q^2/\Lambda^2}\right) \ , \tag{4}$$

where Q^2 is the renormalization scale, Λ is the QCD scale parameter, and N_f is the number of flavors. We take the factorization scale in the structure functions to be $2m_c$ and we consider the renormalization scales $Q=m_c$ and $Q=2m_c$. For the mass of the charm quark we use $m_c=1.5$ GeV. We do not consider the factorization scale below $2m_c$ because the structure functions have been measured only for $Q^2 \geq 8.5$ GeV [8]. In our calculation we use two-loop-evolved parton structure functions: (1) Martin, Roberts, and Stirling, MRS S0 [9], with $\lambda_5=140$ MeV; (2) Martin, Roberts, and Stirling, MRS D0 [9], with $\lambda_5=140$ MeV; (3) Martin, Roberts, and Stirling, MRS D- [9], with $\lambda_5=140$ MeV and "singular" behavior of the gluon distribution at small x, i.e., $G(x,Q^2) \sim x^{-1.5}$; (4) Martin, Roberts, and Stirling, MRS A [10], with $\lambda_5=151$ MeV and "singular" behavior of the gluon distribution at small x, i.e., $G(x,Q^2) \sim x^{-1.08}$. This is the most recent MRS set, adjusted to fit recent H1 and ZEUS data [8].

In Fig. 1 we present our results for the total cross section for charm production in proton-proton collisions for the beam energies ranging from 50 GeV up to 2 TeV. The results were obtained using two different sets of structure functions, MRS D0 (dashed lines) and MRS A (solid lines). We find the uncertainty due to the choice of structure function to be only few percent. This is not surprising because the range of x probed by charm quark pair

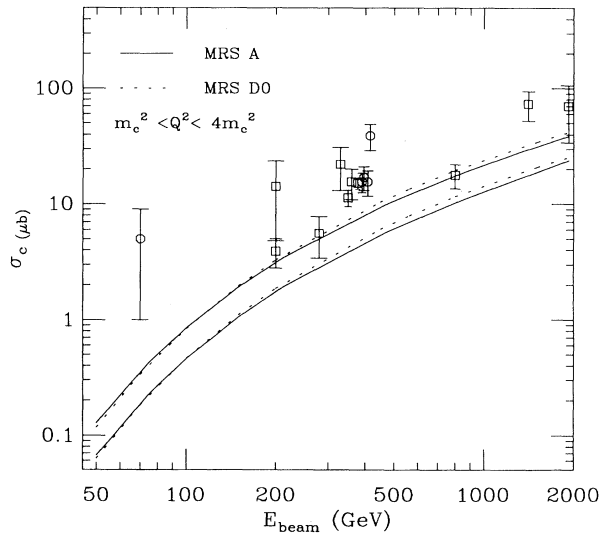

FIG. 1. The total cross section for charm quark production in proton-proton collisions calculated to the next-to-leading order (LO+NLO) for values of E_{beam} ranging from 50 GeV to 2 TeV for two renormalization scales, $Q=m_c$ and $2m_c$. The results are compared to the data from p-p and p-A collisions [11].

production at these energies is well within the range of the data for nucleon structure functions. The top two curves in Fig. 1 correspond to the calculation using the renormalization scale $Q^2 = m_c^2$ and the bottom two to $Q^2 = 4m_c^2$. Comparison of our results with low-energy data for p-p and p-A collisions [11] indicate better agreement for the choice of the renormalization scale $Q^2 = m_c^2$. Future high-precision charm experiments at Fermilab [3] might be able to provide a tighter constraint on this theoretical parameter.

We find that the contribution from higher-order corrections $[O(\alpha_s^3)]$ are important at low energies, especially near the threshold energy for charm production. The K factor, defined as a ratio of the next-to-leading order result to the leading-order one, ranges from about 3.7 at $E_{\rm beam} = 50$ GeV to about 2.2 at $E_{\rm beam} = 2$ TeV.

We predict that the total cross section for charm production in p-p collisions is 180–210 μb (for $Q^2 = m_c^2$) and 112–126 μb (for $Q^2 = 4m_c^2$) at RHIC and 2.4–15.3 mb (for $Q^2 = m_c^2$) and 1.4–9.2 mb (for $Q^2 = 4m_c^2$) at LHC. The range of the cross sections correspond to different structure functions. At RHIC energies, we find that the cross section depends weakly on the choice of the structure function. The average x value that is probed with charm production at $\sqrt{s} = 200$ GeV is on the order of 10^{-2}, still within the range of x for which there is deep-inelastic-scattering data. Theoretical uncertainty due to the choice of the structure function is about 15%. At LHC energies ($\sqrt{s} = 7$ TeV) the average x value probed with charm production in the central rapidity region is about 5×10^{-6}, far below the x range covered by the current deep-inelastic-scattering data. Different sets of structure functions [9,10], which all fit the current data[1] have a different extrapolation to the low-x region. For example, the MRS D- and MRS A gluon distribution have singular behavior in the small-x region, in contrast to MRS D0 and MRS S0 sets. As a consequence, the total cross section for charm production at LHC calculated with MRS D- parton distributions is larger than the one obtained with MRS D0 set by about a factor of 6. We find the K factor for the total cross section for charm production to be between 2 and 2.1 at RHIC and between 2.3 and 2.8 at LHC. The range for the K factor corresponds to the choice of the renormalization scale.

III. CHARM PRODUCTION IN NUCLEAR COLLISIONS

A. Nuclear geometry

Assuming the validity of factorization theorems in the calculation of the cross section for charm production in nuclear collisions, the total number of charm quark pairs produced in A-A collisions at some fixed impact parameter is given by [12]

$$N_c^{AA}(s,b) = \int d^2b_1 dx_a dx_b \sum_{i,j}^{\rm partons} [F_i^A(x_a, Q^2, |\vec{b} - \vec{b}_1|) F_j^A(x_b, Q^2, |\vec{b}_1|) \hat{\sigma}_{i,j}(\hat{s}, m_c^2)] \ , \quad (5)$$

where the $F_i^A(x, Q^2, b)$ is the parton distribution function in a nucleus. We assume that the parton density in a nucleus can be factorized in terms of the (usual) parton structure function modified by the medium effects, $F_i^A(x, Q^2)/A$, and the spatial distribution of partons at some impact parameter b, $T_A(b)$, i.e.,

$$F_i^A(x, Q^2, b) \approx [F_i^A(x, Q^2)/A] T_A(b) \ . \quad (6)$$

The nuclear thickness function, $T_A(b)$, is the number of nucleons per unit transverse area at fixed impact parameter. The spatial (impact parameter) integration that appears in Eq. (5) gives the number of nucleon-nucleon collisions per unit of transverse area at fixed impact parameter, $T_{AA}(b)$, which is related to the nuclear density in the following way [13]:

$$T_{AA}(b) = \int d^2b_1 T_A(|\vec{b}_1|) T_A(|\vec{b} - \vec{b}_1|) \ , \quad (7)$$

where the nuclear thickness function, $T_A(b)$, is the nuclear density integrated over the longitudinal size, i.e.,

$$T_A(b) = \int_{-\infty}^{\infty} dz \, \rho_A(\sqrt{b^2 + z^2}) \ . \quad (8)$$

For A-A collisions we take the nuclear density to be the Woods-Saxon distribution [7] given by

$$\rho(r) = \frac{n_0}{[1 + e^{(r - R_A)/d}]} \ , \quad (9)$$

where $n_0 \approx 0.17/\text{fm}^3$, R_A is the nuclear radius, and $d = 0.54$ fm is the "skin" thickness of this distribution. The density and the nuclear overlapping function are normalized so that $\int d^3r \rho(r) = A$ and $\int d^2b T_{AA}(b) = A^2$. For central collisions the overlapping function can be approximated by $T_{AA}(0) = A^2/\pi R_A^2$, which gives $T_{\rm Au-Au}(0) = 30.7\ \text{mb}^{-1}$.

The nuclear density that is most widely used in the literature is the Gaussian distribution

$$\rho(r) = \frac{A}{\pi^{3/2} a^3} e^{-r^2/a^2} \ , \quad (10)$$

[1]The most recent H1 and ZEUS data on structure functions at low x and low Q^2 [8] are best fitted with MRS A distributions. The data seem to be steeper functions of x than the MRS D0 structure functions and not as steep as the MRS D- [9,10].

where a is related to the charge radius of the nucleus, $\frac{3}{2}a^2 = \langle R_A^2 \rangle$. Functions $T_A(b)$ and $T_{AA}(b)$ can be obtained analytically and are given by

$$T_A(b) = \frac{A}{\pi a^2} e^{-b^2/a^2} \tag{11}$$

and

$$T_{AA}(b) = \frac{A^2}{2\pi a^2} e^{-b^2/2a^2} \ . \tag{12}$$

The formalism for proton-nucleus collisions is similar. The thickness function of the proton is approximated by

$$T_p(b) \simeq \frac{1}{(2\pi)^2} \int d^2k_\perp G_E(k_\perp^2) e^{i\mathbf{k}_\perp \cdot \mathbf{b}} \ , \tag{13}$$

where G_E is the proton electric form factor

$$G_E(k_\perp) \simeq \left(1 + \frac{k_\perp^2}{\nu^2}\right)^{-2} \ . \tag{14}$$

The corresponding overlapping function is given by [14]

$$T_{pA}(b) = \frac{\nu^2 A}{48\pi a^2} \int_0^\infty db' b' e^{-(b^2+b'^2)/a^2} (\mu b')^3 K_3(\mu b') I_0\left(\frac{2bb'}{a^2}\right) \ , \tag{15}$$

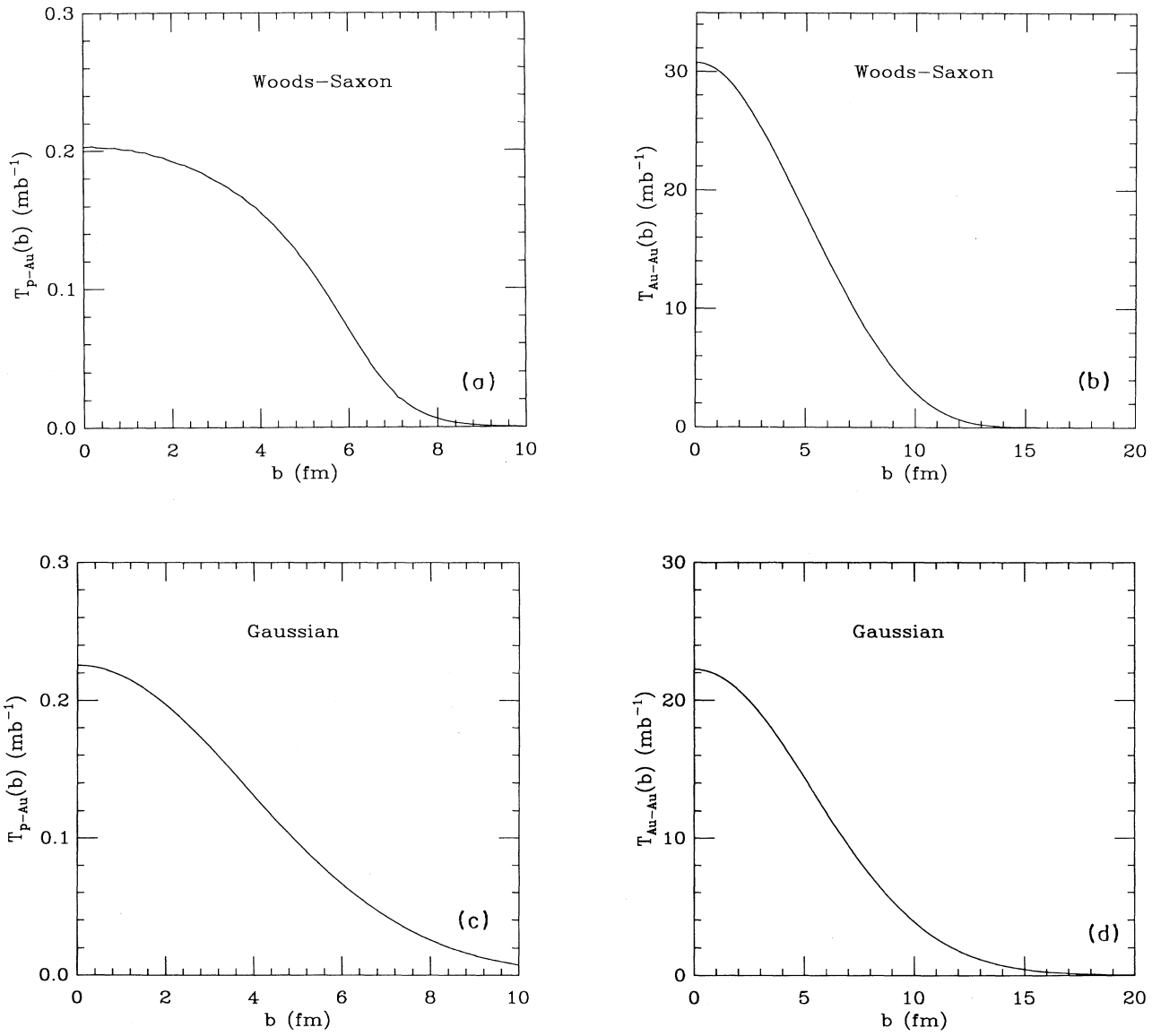

FIG. 2. The nuclear overlapping functions, $T_{AB}(b)$ for p-Au and Au-Au collisions obtained with two different nuclear density functions, (a),(b) Woods-Saxon [7] and (c),(d) the Gaussian form.

where $\nu^2 \simeq 0.71$ (GeV)^2. The expression for T_{pA} derived from a Woods-Saxon distribution cannot be obtained analytically. In Fig. 2, we present $T_{p-\mathrm{Au}}(b)$ and $T_{\mathrm{Au}-\mathrm{Au}}(b)$ obtained with Woods-Saxon and with the Gaussian nuclear density distributions. Although the Gaussian distribution is widely used, the corresponding overlapping function has a long tail and at high energies gives a total inelastic cross section that violates unitarity (i.e., the cross section is larger than the size of the physical system).

B. The nuclear shadowing effect

Calculation of the charm production in nuclear collisions requires knowledge of the nucleon structure function *in-medium*, $F_i^A(x,Q^2)/A$, introduced in Eq. (6). If nucleons were independent parton densities in a nucleus, $F_i^A(x,Q^2)$, would be simply given as A times the parton density in a nucleon. However, at high energies, the parton densities become so large that the sea quarks and gluons overlap spatially and the nucleus cannot be viewed as a collection of uncorrelated nucleons. This happens when the longitudinal size of the parton, in the infinite momentum frame of the nucleus, becomes larger than the size of the nucleon. Partons from different nucleons start to interact and through annihilation effectively reduce the parton density in a nucleus. When partons inside the nucleus completely overlap, they reach a saturation point. Motivated by this simple parton picture of the nuclear shadowing effect and taking into account the $A^{1/3}$ dependence obtained by considering the modified, nonlinear Altarelli-Parisi equations with gluon recombination included, the modifying factor to the parton structure function in a nucleus can be written as [15]

$$R(x,A) \equiv \frac{F_i^A(x,Q^2)}{AF_i^N(x,Q^2)} = \begin{cases} 1-\frac{3}{16}x+\frac{3}{80}, & 0.2 < x \le 1 \\ 1, & x_n < x \le 0.2 \\ 1-D(A^{1/3}-1)\frac{1/x-1/x_n}{1/x_A-1/x_n}, & x_A \le x \le x_n \\ 1-D(A^{1/3}-1), & 0 < x < x_A \end{cases} \tag{16}$$

where $F_i^N(x,Q^2)$ is the parton structure function in a nucleon, x_n is the value of x which specifies the onset of the shadowing effect [$x_n = 1/(2r_p m_p) \approx 0.1$], x_A corresponds to the saturation point [$x_A = 1/(2R_A m_p)$], m_p is the mass of the proton, r_p is the radius of a proton, and R_A is the radius of the nucleus. It is important to note that x_n is fixed for *all* nuclei, and x_A can be determined for each nucleus. Thus, the only parameter that is free to be fitted is D. In Fig. 3, we plot $R(x,A)$ given by Eq. (16) by fitting D to deep-inelastic lepton-nucleus data on the ratio $F_2^A(x,Q^2)/F_2^D(x,Q^2)$ [16]. We find that $R(x,A)$ has a much steeper x dependence than the data, especially for $0.002 \le x \le 0.1$, the region of relevance to charm production at RHIC and LHC energies. Even the best fit overestimates the observed shadowing effect by about 15%. Consequently charm production calculated with this shadowing function would be underestimated by about 40%.

At low energies, the effect from shadowing is ranging from 3% at $E_{\mathrm{beam}} = 50$ GeV to 6% at $E_{\mathrm{beam}} = 2$ TeV in p-Au collisions and from 6% at $E_{\mathrm{beam}} = 50$ GeV to 13% at $E_{\mathrm{beam}} = 2$ TeV in Au-Au collisions. This effect is even smaller for a lighter nucleus. The reason that the nuclear shadowing effect is so small is due to the fact that the x region probed by charm production at these energies is $0.05 \le x \le 1$, not too far from the value for the onset of shadowing, $x_n \approx 0.1$.

Recently, a new parametrization of the nuclear shadowing function given by [17]

$$R(x,A) = \begin{cases} \alpha_3 - \alpha_4 x, & x_0 < x \le 0.6, \\ (\alpha_3 - \alpha_4 x_0)\frac{1+k_q\alpha_2(1/x-1/x_0)}{1+k_q A^{\alpha_1}(1/x-1/x_0)}, & x \le x_0, \end{cases} \tag{17}$$

has been proposed. This new function gives much better description of all EMC, NMC, and E665 data [16] than the shadowing function of Eq. (16). This is illustrated in Fig. 3. The parameters, k_q, α_1, α_2, α_3, and x_0 are fitted to deep-inelastic data for the ratio $F_2^A(x,Q^2)/F_2^D(x,Q^2)$ [16] and can be found in Ref. [17]. In our calculation of charm production in p-Au and Au-Au collisions we use the nuclear shadowing function given by Eq. (17).

Presently there is no theory which can quantitatively describe the observed nuclear shadowing effect [16]. Recent calculations of the perturbative gluon shadowing seem to substantially underestimate the observed effect, indicating perhaps that the nonperturbative effects are large and cannot be neglected [18]. Better understanding of the nuclear shadowing effect might require a novel, nonperturbative approach.

To obtain the effective A dependence of the total inclusive charm cross section in nuclear collisions, defined as $\sigma_c^{AA} = A^{\alpha_{\mathrm{eff}}}\sigma_c^{pp}$, we use the total charm cross section in hadronic collisions at $\sqrt{s} = 200$ GeV ($\sqrt{s} = 7$ TeV) to be $\sigma_c^{pp} = 180$ μb ($\sigma_c^{pp} = 2.4$ mb). The corresponding α_{eff} for central (inelastic) Au-Au collisions is 1.27 (1.94) at RHIC and 1.2 (1.87) at the LHC.

To be able to determine the fraction of central or inelastic events which contain at least one charm quark pair, we need to consider the semiclassical probability of having at least one parton-parton collision at fixed impact parameter, $1 - e^{-N_c(b)}$, where $e^{-N_c(b)}$ is the probability that there is *no* parton-parton scattering in Au-Au collision at impact parameter b. The fraction of events in Au-Au collisions that contain at least one charm quark pair is then given by

$$\frac{\sigma_c^{AA}}{\sigma_{\mathrm{inelastic}}^{AA}} = \frac{\int d^2b\{1-\exp[-N_c(b)]\}}{\int d^2b\{1-\exp[-T_{AA}(b)\sigma_{\mathrm{in}}^{pp}]\}}, \tag{18}$$

where N_c is given by Eq. (5).

To determine the fraction of all *central* events that contain at least one charm quark pair we integrate Eq. (18) over a small range of impact parameters, i.e., $0 \le b \le 0.1$ fm. We find that 98% (99%) of central events at RHIC (LHC) energies will contain at least one charm quark pair. For *inelastic* collisions we integrate Eq. (18) over

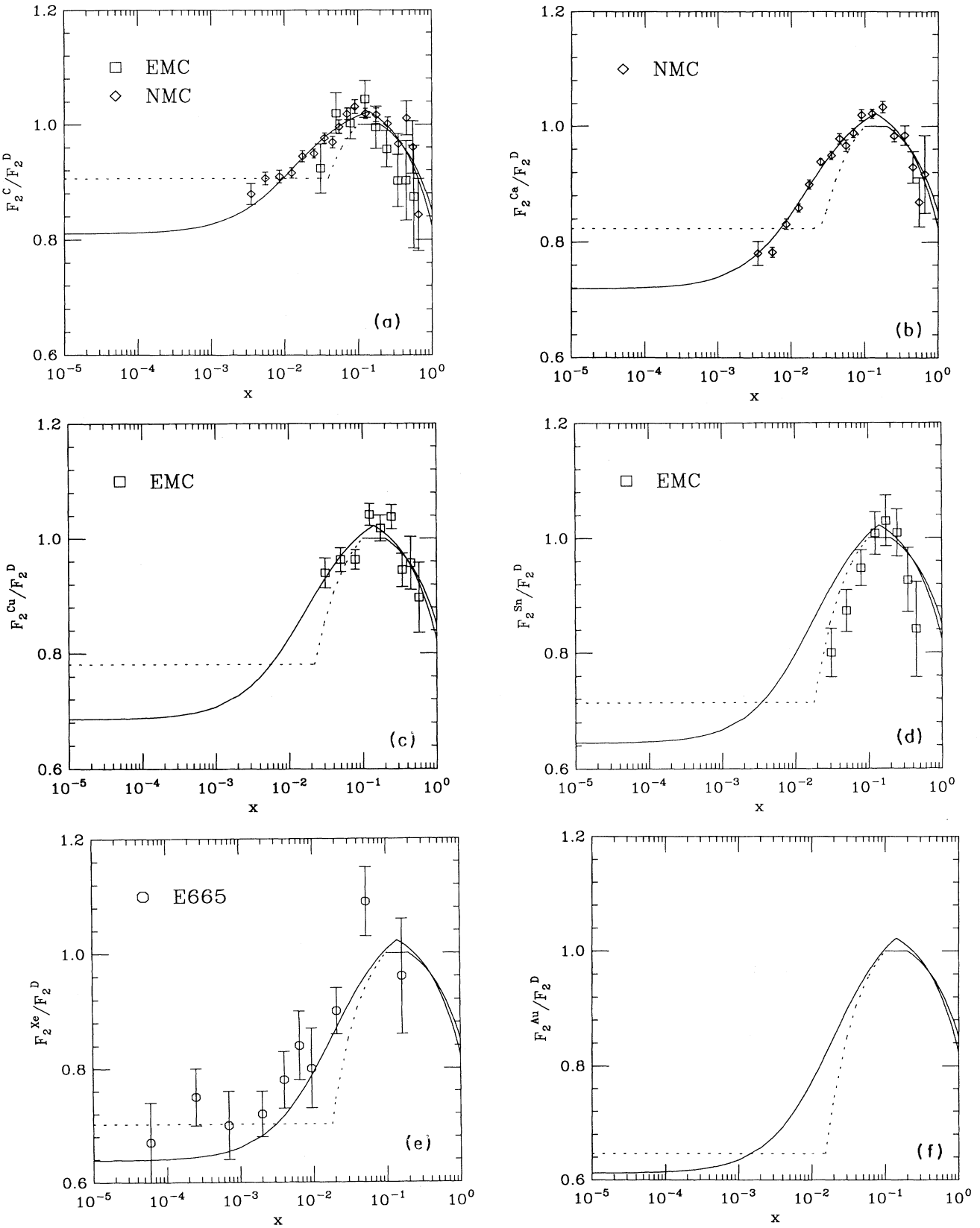

FIG. 3. The nuclear shadowing functions given by Eq. (17) (solid line) and by Eq. (16) (dashed line) fitted to the EMC, NMC, and E665 deep-inelastic lepton-nucleus data [16]. We include a plot of the nuclear shadowing function for Au given by Eq. (17) (solid line), which is used in our calculation of charm production in p-Au and Au-Au collisions.

all impact parameters and find this fraction to be 38% at RHIC and ranging from 54 to 72% at the LHC. Note that the integrated charm cross section in Eq. (18) includes multiple independent parton-parton scatterings which means multiple charm quark pair production.

IV. RAPIDITY AND TRANSVERSE MOMENTUM DISTRIBUTIONS FOR CHARM PRODUCTION IN *p*-*p*, *p*-Au, AND Au-Au COLLISIONS

In the previous section we have seen that the nuclear shadowing function depends on the kinematic variable x. Thus, it seems plausible that the effect that nuclear shadowing has on charm production is not uniform throughout all of phase space. Furthermore, the new subprocesses that are part of the next-to-leading order calculation have different contributions in different regions of phase space. Thus, by studying the single-differential distributions one might be able to get more information about the underlying dynamics of charm production in nuclear collisions.

In general, the single-differential distribution is obtained by integrating the double-differential inclusive distribution

$$\frac{dN_c}{d^2p_T dy} = T_{AA}(0)\frac{d\sigma_c}{d^2p_T dy}, \tag{19}$$

where the double-differential inclusive cross section per nucleon-nucleon interaction *in medium* is given by

$$\frac{d\sigma_c}{d^2p_T dy} = \sum_{i,j}^{\text{partons}} \int dx_a dx_b \frac{F_i^A(x_a,Q^2)}{A}\frac{F_j^A(x_b,Q^2)}{A}\frac{d\hat{\sigma}_{i,j}(Q^2,m_c,\hat{s})}{d^2p_T dy}. \tag{20}$$

The parton differential cross section calculated to $O(\alpha_s^3)$ can be written as [2]

$$\frac{d\hat{\sigma}_{i,j}}{d^2p_T dy} = \frac{\alpha_s^2}{\hat{s}}h_{i,j}^{(0)} + \frac{\alpha_s^3}{2\pi\hat{s}^2}h_{i,j}^{(1)}. \tag{21}$$

Expressions for the functions $h_{i,j}^{(0)}$ and $h_{i,j}^{(1)}$ can be found in Ref. [2].

We obtain the rapidity and transverse momentum distribution for charm production in *p*-*p*, *p*-Au, and Au-Au collisions by integrating the Eq. (20) over the appropriate variable [i.e., to obtain the rapidity distribution, for example, we integrate Eq. (20) over the transverse momentum]. We use two different choices of the renormalization scale, as in the case of the total cross section, and three different structure functions: MRS D0, MRS D-, and MRS A [9,10].

In Fig. 4, we present our results for the rapidity distribution for charm production at RHIC. We find that different choice of the structure function result in about 8% uncertainty at $y = 0$, while at $y = 3$ this uncertainty is almost 40%. This is due to the fact that charm production in the large rapidity region is probing smaller x region than in the case when charm quarks are produced in the central rapidity region ($x_{\text{average}} \approx 0.01$ for $y \approx 0$ and $x_{\text{average}} \approx 10^{-5}$ for $y \approx 3$). At LHC energies, the choice of the structure functions introduces a much larger theoretical uncertainty. From Fig. 5, we note that at $y \approx 3$ this uncertainty is about a factor of 7. Furthermore, we find that the shape of the rapidity distribution is sensitive to the low-x behavior of the structure function, resulting in a "dip" at $y = 0$. At $y = 0$, the x values of the incoming partons are approximately 10^{-4}, and therefore both

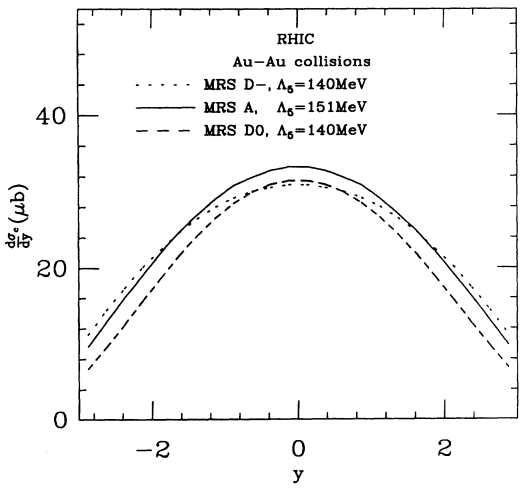

FIG. 4. The rapidity distribution for charm quark production in Au-Au collisions at RHIC energies calculated to $O(\alpha_s^3)$ and with three different sets of structure functions: MRS A (solid line), MRS D- (dotted line), and MRS D0 (dashed line). The renormalization scale is taken to be $Q = m_c$.

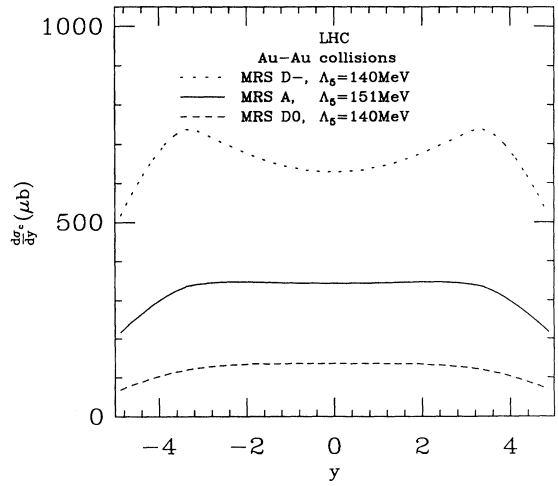

FIG. 5. Same as Fig. 4, but for LHC. The curves are labeled as in Fig. 4.

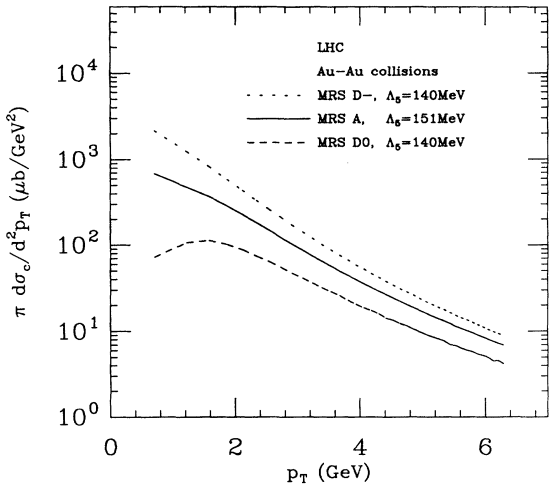

FIG. 6. Same as Fig. 5, but for the transverse momentum distribution. The curves are labeled as in Fig. 5.

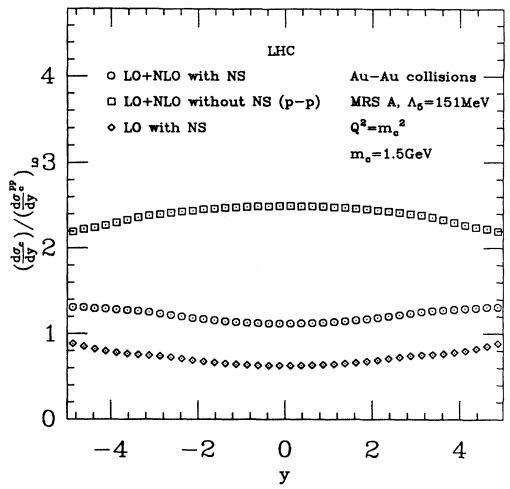

FIG. 8. The *effective* (in-medium) K factor, defined as $K \equiv (d\sigma_c^{AA}/dy)/(d\sigma_c^{pp}/dy)_{\rm LO}$, for the distributions in Fig. 7. The K factor for p-p collisions is about 2.5 (squares), while the K-factor in medium (in case of Au-Au collisions) is about 1.1 (circles) in the central rapidity region.

of the structure functions that appear in the distribution given by Eq. (20) are evaluated in the region of maximum nuclear shadowing. When $y \approx 3.5$, the x region probed is a combination of small x (maximum shadowing) and intermediate x (small shadowing effect) leading to the larger values for the number of charm quarks produced than in the central rapidity region. Furthermore, the combination of the x dependence of nuclear shadowing effect and the steep increase of the structure function at low x could result in less overall shadowing at $y \approx 3.5$. In Fig. 5, we note that this is apparent for the MRS D- structure function, while the effect is much smaller in the case of MRS A and MRS D0 sets. In Fig. 6, we present the results for the transverse momentum distributions for the charm production at LHC. We note that the shape of p_T distribution is sensitive to the choice of the structure function. The p_T distribution is much steeper when obtained with MRS D- structure function than with MRS A or with MRS D0 set. The theoretical uncertainty due to the choice of the structure function is about an order of magnitude at low p_T, where the small-x region is probed, while at larger values of p_T (i.e., $p_T \geq 6$ GeV) this uncertainty is substantially reduced. In Fig. 7, we present the rapidity distribution for charm production at LHC energies calculated with the MRS A parton distribution and with $Q^2 = m_c^2$. The two distributions without nuclear shadowing correspond to p-p collisions. To obtain the number of charm quark pairs produced in Au-Au collisions, we need to multiply the rapidity distribution which contains nuclear shadowing effects (solid line) with

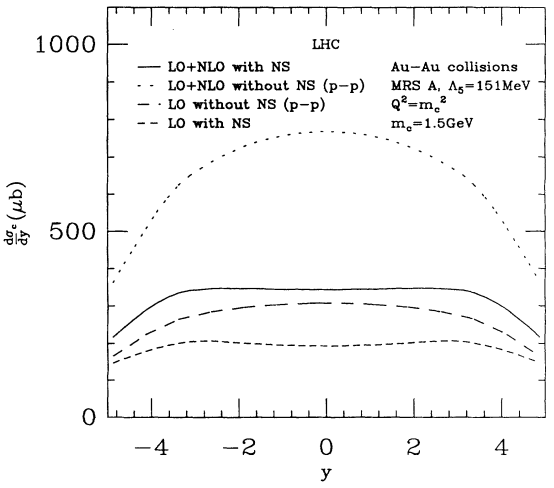

FIG. 7. The rapidity distribution for charm quark production in proton-proton and Au-Au collisions at LHC energies calculated to the next-to-leading order (LO+NLO) with nuclear shadowing effects (NS) (solid line), without NS (i.e., for p-p collisions) (dotted line), only leading-order (LO) (dashed line) and LO without NS (long-dashed line).

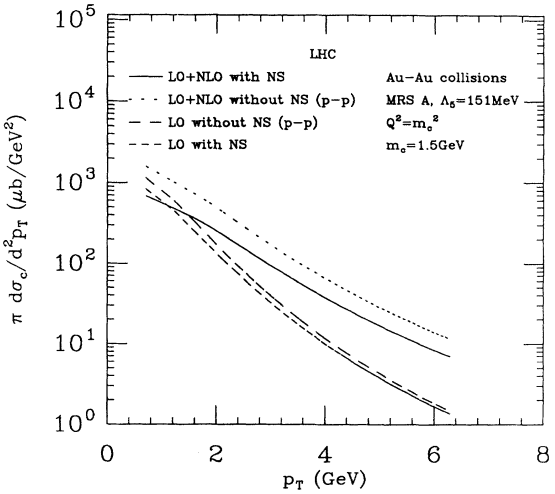

FIG. 9. Same as Fig. 7, but for the transverse momentum distribution. Curves are labeled as in Fig. 7.

the geometrical factor (i.e., the spatial, overlapping function) presented in Fig. 2. To get the number of charm quark pairs produced in central collisions (i.e., at zero impact parameter), for example, one would need to multiply $d\sigma_c/dy$ by $T_{AA}(0)$. We note that rapidity distribution for charm production in Au-Au collisions at LHC obtained with MRS A structure function is flat for $|y| \leq 3$.

The *effective* (in-medium) K factor can be defined in a way analogous to the hadronic K factor, namely as the ratio of a particular distribution for charm production in *nuclear* collisions to the leading-order distribution without any nuclear effects. Thus, this K factor is a measure of the size of the effect due to higher-order corrections *combined* with nuclear effects. In Fig. 8, we present the K factor for the rapidity distributions at LHC energies. We see that over the range $-5 \leq y \leq 5$ the K factor has weak dependence on y. In the central rapidity region, the K factor for Au-Au collisions is about 1.1 (circles), while the hadronic K factor is 2.5 (squares). The results for the hadronic and for the effective K factor for the rapidity and transverse momentum distributions at RHIC energies can be found in Ref. [19].

In Fig. 9, we present results for the transverse momentum distributions at the LHC. The calculation is done using MRS A parton distributions and a renormalization scale $Q^2 = m_c^2$. At low p_T the nuclear shadowing effects suppress charm production by about 62%, while the higher-order corrections, $O(\alpha_s^3)$, enhance the charm production by about 50%, resulting in p_T distribution which is effectively lower than the leading-order result for p-p collisions.[2] At large p_T, we expect nuclear effects to become negligible and the p_T distribution to approach the next-to-leading order results for p-p collisions. In Fig. 10 we present the hadronic and the *effective* K factor for the transverse momentum distribution for charm production at LHC energies. We find that while hadronic K factor varies from 1.4 to 7.6 for $0.7 \leq p_T \leq 6$ GeV, the K factor for Au-Au collisions changes from 0.6 to 4.6 in the same p_T range. For the x_F distribution, we find the *effective* K factor for Au-Au collisions at RHIC (LHC) energies to increase from 1.5 (1.2) at $x_F \approx 0$, to around 5.2 (3) at $x_F \approx 1$, while the hadronic K factor changes from 2 (2.4) at $x_F \approx 0$, to about 6.6 (5) at $x_F \approx 1$.

We present our result for the single-differential distribution in p-A collisions in terms of the parameter $\alpha_{\rm eff}$, defined as

$$\tilde{\sigma}_{AA} = A^{\alpha_{\rm eff}} \tilde{\sigma}_{pp} \ , \tag{22}$$

where $\tilde{\sigma}_{pp}$ is a differential cross section for charm production in hadronic collisions, and $\tilde{\sigma}_{AA}$ is the corresponding cross section in nuclear collisions. The parameter $\alpha_{\rm eff}$ is a sum of the geometrical contribution and the nuclear shadowing effect (i.e., $\alpha_{\rm eff} = \alpha + \alpha_{\rm NS}$, $\alpha_{\rm NS} < 0$). The later effect reduces the value of the "standard" α, which for minimum bias A-A collisions is 2, while for the central A-A collisions, $\alpha = \frac{4}{3}$. The values for $\alpha_{\rm NS} \equiv \alpha_{\rm eff} - \alpha$ in p-A and A-A collisions at RHIC and LHC are presented in Fig. 11. Knowing $\alpha_{\rm eff}(y)$ and $\alpha_{\rm eff}(p_T)$ it is possible to extract the rapidity and the transverse momentum distribution for p-A collisions by suitable modification of the distribution for charm production in p-p collisions. For example, $d\sigma_c^{pA}/dy = A^{\alpha_{\rm eff}(y)}(d\sigma_c^{pp}/dy)$. The K factor for inclusive distribution for charm production in p-A collisions can also be determined from $\alpha_{\rm eff}$, as $K = (d\sigma_c^{pA}/dy)/(d\sigma_c^{pp}/dy)_{\rm LO}$.

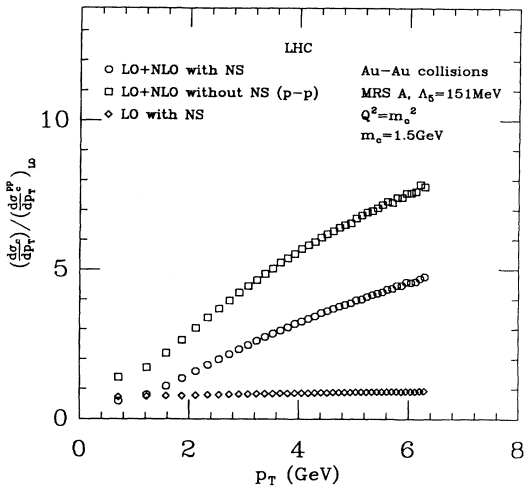

FIG. 10. The same as Fig. 8 but for the transverse momentum distributions presented in Fig. 9. The K factor for p-p collisions ranges from 1.4 at $p_T = 0.7$ GeV to 7.6 at $p_T = 6$ GeV. In the same p_T range, the K-factor in medium increases from 0.6 to 4.6.

V. CONCLUSIONS

To summarize, we have presented results for the differential and total inclusive cross sections for charm production in hadronic and heavy-ion collisions at RHIC and LHC energies. We have included the next-to-leading-order corrections, $O(\alpha_s^3)$, and the nuclear shadowing effect with the assumption that the shadowing effect is the same for the gluon density in a nucleus as the observed effect in the quark distribution [16]. We have shown that low-energy data for the total cross section for charm production in p-p and p-A collisions provide some constraints on out theoretical parameters, especially for the choice of the renormalization scale. The choice $Q = m_c$ seems to be preferred by the data. Theoretical uncertainty in the calculation of charm production in nuclear collisions due to the choice of the structure function is small at Fermilab fixed target energies (only few percent) and at RHIC (8% in the central rapidity region), while at LHC ener-

[2]From Fig. 2 we note that the nuclear shadowing of a parton distribution in gold at $x \leq 10^{-4}$ is about 62%. Therefore, combination of two parton distributions which appears in Eq. (20) results in about 62% overall suppression of charm production at low p_T.

gies this uncertainty is about a factor of 6. Furthermore, the shape of the rapidity distribution for charm production in Au-Au collisions at LHC is very sensitive to the low-x behavior of the gluon structure function, resulting in a larger "dip" at $y = 0$ for a more singular function. Similarly, the transverse momentum distribution at LHC is much steeper when obtained with MRS D- structure function than with less singular structure function, such as MRS A set or the nonsingular structure function, such as MRS D0 set. For the rapidity distribution, we have found the hadronic K factor to be about 2 (2.5) at RHIC (LHC) energies, while the *effective* K factor for Au-Au collisions is about 1.5 (1.1). In case of p_T distribution, the hadronic K factor at LHC energies varies from 1.4 at $p_T = 0.7$ GeV to 7.6 at $p_T = 6$ GeV, while the *effective* K factor changes from 0.6 to 4.6 in the same p_T range. This behavior of the *effective* K factor is a direct consequence of the fact that the low p_T region (or small x) corresponds to the maximum shadowing of the gluon distribution, which in the case of gold is about 62%, while the larger values of p_T probe region of phase space where the nuclear shadowing is smaller. We have also obtained the effective A dependence for the differential and total cross sections for charm production p-Au collisions at RHIC and in Au-Au collisions at the LHC. We have found that the dominant contribution to charm produc-

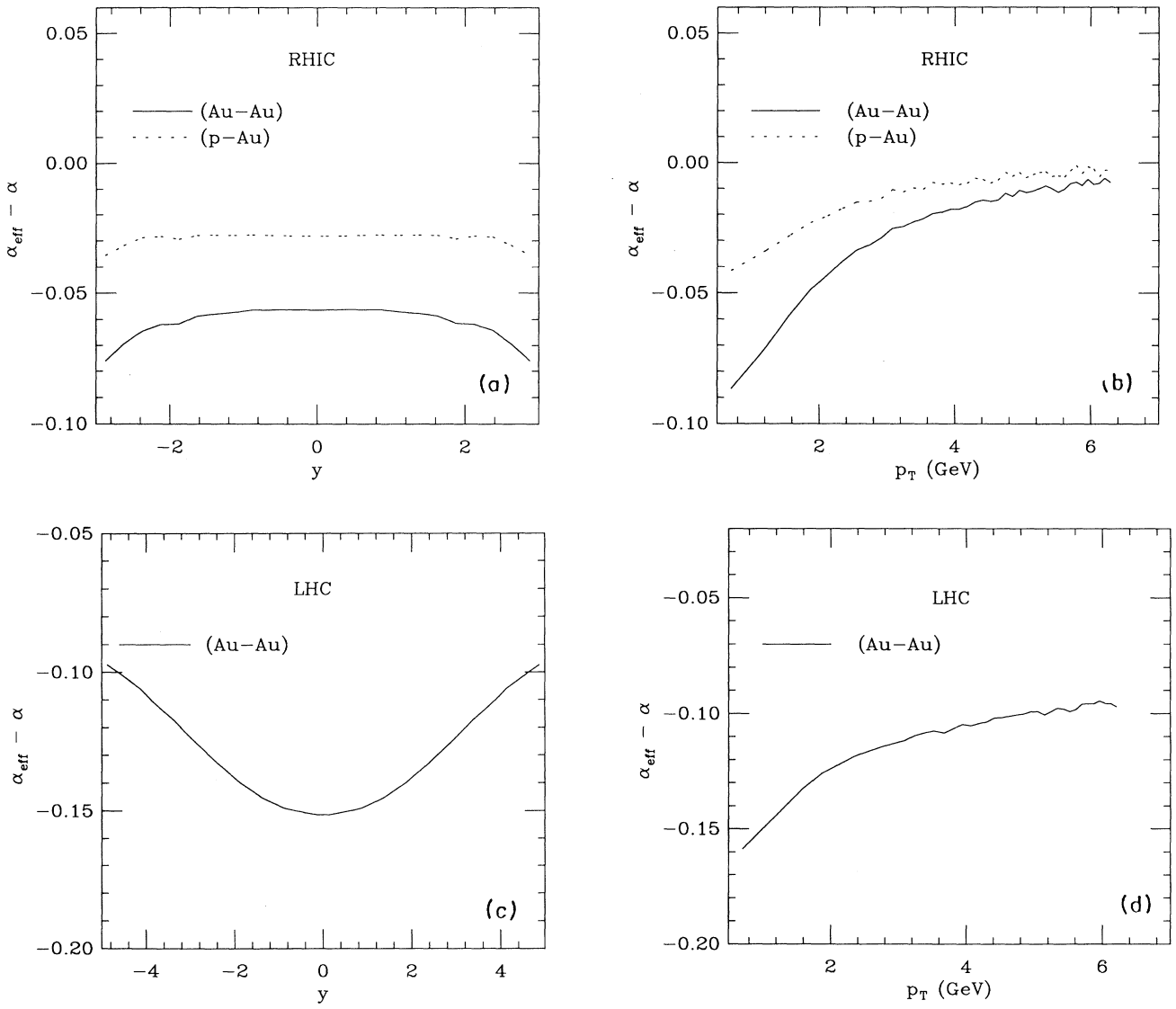

FIG. 11. The plot of $\alpha_{\rm eff} - \alpha$ as a function of y and p_T for p-Au and Au-Au collisions. The $\alpha_{\rm eff}$ is defined as $\tilde{\sigma}_{\rm Au-Au/p-Au} = A^{\alpha_{\rm eff}} \tilde{\sigma}_{p-p}$, where $\tilde{\sigma}_{p-p}$ is a differential cross section for charm production in p-p collisions and $\alpha_{\rm eff} = \alpha + \alpha_{\rm NS}$. The parameter α, frequently used in the literature, corresponds to the A dependence coming from the geometry only. In the limit of no nuclear shadowing, $\alpha_{\rm eff} \to \alpha$. In case of central A-A collisions, $\alpha = \frac{4}{3}$, while for minimum bias collisions $\alpha = 2$. For p-A minimum bias collisions, $\alpha = 1$.

tion comes from the initial state gluons (about 95% at RHIC and 99% at LHC). Thus, combined measurements of inclusive charm production in hadronic and nuclear collisions at these energies, in addition to providing an important test of perturbative QCD in the small-Q^2 and small-x region, might be able to provide valuable information about the elusive role of gluons inside a nucleus, especially in the region of very small x.

ACKNOWLEDGMENTS

We would like to thank M. Mangano and P. Nason for providing us with the Fortran routines for calculating double differential distributions for charm production in hadronic collisions. This work was supported in part through U.S. Department of Energy Grants Nos. DE-FG03-93ER40792 and DE-FG02-85ER40213.

[1] P. Nason, S. Dawson, and R. K. Ellis, Nucl. Phys. **B327**, 49 (1989); **B303**, 607 (1988).

[2] M. L. Mangano, P. Nason, and G. Ridolfi, Nucl Phys. **B373**, 295 (1992).

[3] For a review of the future plans for high-precision charm measurements see Proceedings of the Workshop on the Future of High Sensitivity Charm Experiments: CHARM2000, Batavia, IL, 1994 (unpublished).

[4] E. Shuryak, Phys. Rev. Lett. **68**, 3270 (1992); K. Geiger, Phys. Rev. D **48**, 4129 (1993).

[5] For example, see B. Muller, in *Particle Production in Highly Excited Matter*, edited by H. Gutbrod and J. Rafelski (Plenum, New York, 1993).

[6] For a recent review of the thermal photons and dileptons see V. Ruuskanen, Proceedings of Quark Matter '90 [Nucl. Phys. **A525**, 255c (199)]; and on J/ψ suppression see S. Gavin, in Proceedings of the Second International Conference on Physics and Astrophysics of Quark Gluon Plasma, Calcutta, 1993 (in press).

[7] A. Bohr and B. R. Mottelson, *Nuclear Structure I* (Benjamin, New York, 1969), p. 160.

[8] For a recent review of the structure functions and HERA physics see G. Wolf, DESY Report No. DESY 94-022.

[9] A. D. Martin, W. J. Sterling, and R. G. Roberts, Phys. Rev. D **47**, 867 (1993).

[10] A. D. Martin, W. J. Sterling, and R. G. Roberts, RAL Report No. RAL-94-055.

[11] S. Aoki *et al.*, Phys. Lett. B **224**, 441 (1989); S. P. K. Tavernier, Rep. Prog. Phys. **50**, 1439 (1987); S. Barlag *et al.*, Z. Phys. C **39**, 451 (1988).

[12] For a recent review of the factorization theorems in perturbative QCD see J. C. Collins, D. E. Soper, and G. Sterman, in *Perturbative Quantum Chromodynamics*, edited by A. H. Mueller (World Scientific, Singapore, 1989).

[13] K. J. Eskola, K. Kajantie, and J. Lindfors, Nucl. Phys. **B323**, 37 (1989).

[14] L. Durand and H. Pi, Phys. Rev. D **38**, 78 (1988).

[15] J. Qiu, Nucl. Phys. **B291**, 746 (1987); K. J. Eskola, *ibid.* **B400**, 240 (1993).

[16] P. Amaudruz *et al.*, NMC Collaboration, Z. Phys. C **51**, 387 (1991); M. R. Adams *et al.*, E665 Collaboration, Phys. Rev. Lett. **68**, 3266 (1992); J. Ashman *et al.*, EMC Collaboration, Phys. Lett. B **202**, 603 (1988); M. Arneodo *et al.*, *ibid.* **211**, 493 (1988).

[17] C. J. Benesh, J. Qiu, and J. P. Vary, Los Alamos Report No. LA-UR-94-784.

[18] K. J. Eskola, J.-W. Qiu, and X.-N. Wang, Phys. Rev. Lett. **72**, 36 (1994).

[19] I. Sarcevic and P. Valerio, Phys. Lett. B **338**, 426 (1994).